nature materials

LETTERS

https://doi.org/10.1038/s41563-019-0324-5

Emissive and charge-generating donor–acceptor interfaces for organic optoelectronics with low voltage losses

Sascha Ullbrich[1,5*], Johannes Benduhn[1,5*], Xiangkun Jia[1,5], Vasileios C. Nikolis[1], Kristofer Tvingstedt[2], Fortunato Piersimoni[3], Steffen Roland[3], Yuan Liu[1], Jinhan Wu[1], Axel Fischer[1], Dieter Neher[3], Sebastian Reineke[1], Donato Spoltore[1] and Koen Vandewal[1,4*]

Intermolecular charge-transfer states at the interface between electron donating (D) and accepting (A) materials are crucial for the operation of organic solar cells but can also be exploited for organic light-emitting diodes[1,2]. Non-radiative charge-transfer state decay is dominant in state-of-the-art D–A-based organic solar cells and is responsible for large voltage losses and relatively low power-conversion efficiencies as well as electroluminescence external quantum yields in the 0.01–0.0001% range[3,4]. In contrast, the electroluminescence external quantum yield reaches up to 16% in D–A-based organic light-emitting diodes[5–7]. Here, we show that proper control of charge-transfer state properties allows simultaneous occurrence of a high photovoltaic and emission quantum yield within a single, visible-light-emitting D–A system. This leads to ultralow-emission turn-on voltages as well as significantly reduced voltage losses upon solar illumination. These results unify the description of the electro-optical properties of charge-transfer states in organic optoelectronic devices and foster the use of organic D–A blends in energy conversion applications involving visible and ultraviolet photons[8–11].

Optical or electrical excitation at organic electron-donating–electron-accepting (D–A) interfaces results in the formation of charge-transfer (CT) states, where the electron almost fully resides on A and the hole on D[12]. The decay of an excited CT state regenerates a neutral ground state, a process ideally accompanied by the emission of a photon with an energy below the optical gaps (E_{opt}) of both D and A. When used for organic light-emitting diodes (OLEDs)[6,13,14], such emission from intermolecular excitations is often termed exciplex emission[2,15,16]. In organic solar cells (OSCs), a similar type of intermolecular CT state has been shown to be essential for the efficient generation of free charge carriers upon illumination[17,18]. The energy of the CT state (E_{CT}) has been demonstrated to limit the open-circuit voltage (V_{oc}) and, consequently, the overall photovoltaic power conversion efficiency (PCE)[19]. Typically, the difference between E_{CT} and eV_{oc} (where e is the elementary charge) is ~0.2–0.3 eV higher than for inorganic and perovskite-based technologies, the reason being the dominance of non-radiative decay pathways causing additional voltage losses (ΔV_{nr})[3,20]. In this respect, the photovoltage of OSCs would benefit substantially by approaching the high electroluminescence (EL) external quantum yield (EQE_{EL}) values reported for the technically akin visible-light-emitting D–A blends[6]. It is therefore crucial to better understand which molecular and microstructural properties are responsible for the emissive and charge-generating nature of those organic D–A interfaces. In this work, we study archetypical D–A combinations, as reported for OLEDs and OSCs. In both cases, we detect intermolecular CT emission, but also CT absorption originating from the same manifold of intermolecular states. We demonstrate that equilibrium between CT states and free charge carriers is a necessary requirement to achieve a good photovoltaic performance, which moreover also results in low turn-on voltages for electroluminescence. For the visible-light-emitting and comparably efficient D–A blends ($EQE_{EL} > 1\%$), we observe a severe reduction of ΔV_{nr}, reaching values between 0.09 and 0.13 V, more than 0.15 V lower than typical values (0.25–0.35 V) in the currently highest performing OSC blends[3]. We attribute these strongly reduced losses to an increased E_{CT}, effectively suppressing non-radiative decay by reducing electron–phonon coupling. This opens up perspectives for organic materials to efficiently convert the energy of visible and ultraviolet photons, for example for applications in smart, UV–vis absorbing windows[8], photovoltaic devices for indoor applications[9] or high-voltage multijunction OSCs[10,11].

We characterize the OSC performance for a typical OSC (DCV5T-Me:C_{60})[10] and two CT-OLEDs (BF-DPB:TmPPPyTz and BF-DPB:B4PYMPM). Due to their high E_{opt}, the photocurrent of the CT-OLEDs under solar illumination is much lower than for DCV5T-Me:C_{60}. For chemical structures and photovoltaic performance, see Fig. 1a,e–g; the energy levels are listed in Supplementary Table 5. The peak value of the photovoltaic external quantum efficiency (EQE_{PV}) of the BF-DPB based devices is about 31% (B4PYMPM as A) and 18% (TmPPPyTz as A), while it is 75% for DCV5T-Me:C_{60} (Supplementary Fig. 1a,b). Fill factors (FFs) of 65% and 70% are achieved for DCV5T-Me:C_{60} and BF-DPB:B4PYMPM, while the FF for BF-DPB:TmPPPyTz is much lower (<42%). The peak of electroluminescence is at 2.14 eV for both BF-DPB-based blends, with EQE_{EL} values of 1.5% and 2.6%, respectively, while the peak emission for DCV5T-Me:C_{60} is ~1 eV lower with an EQE_{EL} of 0.0006%. The V_{oc} at 1 sun illumination intensity of the CT-OLEDs is very high—2.04 V and 2.13 V, respectively—approaching the

[1]Dresden Integrated Center for Applied Physics and Photonic Materials (IAPP) and Institute for Applied Physics, Technische Universität Dresden, Dresden, Germany. [2]Experimental Physics VI, Julius-Maximilian University of Würzburg, Würzburg, Germany. [3]Institute of Physics and Astronomy, University of Potsdam, Potsdam, Germany. [4]Present address: Institute for Materials Research (IMO-IMOMEC), Hasselt University, Diepenbeek, Belgium. [5]These authors contributed equally: Sascha Ullbrich, Johannes Benduhn, Xiangkun Jia. *e-mail: sascha.ullbrich@tu-dresden.de; johannes.benduhn@tu-dresden.de; koen.vandewal@uhasselt.be

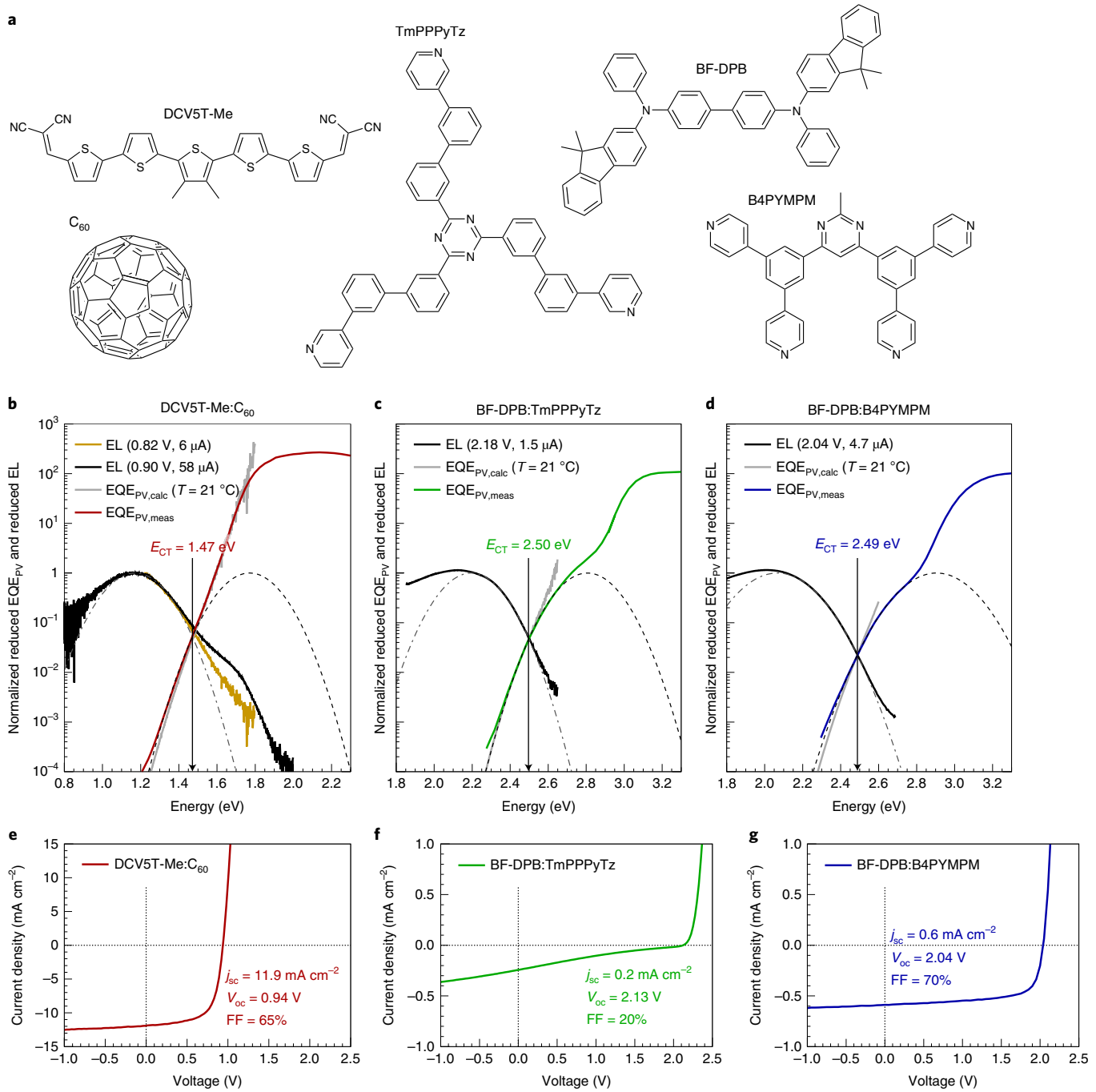

Fig. 1 | Studied material systems, reciprocity relation between CT absorption and emission, and current–voltage characteristics. a, Chemical structures of the investigated material systems. **b**–**d**, Normalized reduced electroluminescence (EL) and EQE_{PV} spectra as a function of the photon energy for three exemplary devices. The electroluminescence was measured using low injection currents to ensure that the charge carriers reach thermal equilibrium before recombination. The light grey line shows an excellent agreement of the calculated EQE_{PV} spectrum under the assumption of reciprocity between absorption and emission, and the measured EQE_{PV}. Dashed curves show Gaussian fits to either the electroluminescence or the EQE_{PV} spectra, following the method outlined in ref. [19]. The crossing point between the appropriately scaled EQE_{PV} and electroluminescence represents E_{CT}, highlighted by vertical black arrows. In **b**, results are shown for a well performing OSC consisting of DCV5T-Me as D and C_{60} as A; the electroluminescence is shown for two different injection currents to better cover the full spectral range, where only the low-injection curve was used to analyse the reciprocity. In **c** and **d**, results are shown for devices made of typical CT-OLED materials: BF-DPB:TmPPPyTz and BF-DPB:B4PYMPM, respectively. **e**–**g**, Corresponding current–density voltage curves measured under simulated AM1.5G solar illumination.

equivalent energy of the emission peak and indicating exceptionally low voltage losses for these devices. For all three devices, we sensitively measure the EQE_{PV} and electroluminescence spectra, revealing distinct low-energy absorption and emission features, below the E_{opt} of the constituting neat D and A materials (Fig. 1b–d). In all cases, the measured absorption and emission spectra obey the reciprocity relation that connects both quantities[19,21], thereby proving that both absorption and emission originate from the same

electronic state, the CT state. Therefore, the term exciplex should be avoided to denote this state, because its original definition implies the absence of a stable ground state and corresponding characteristic absorption band[16,22].

We investigate additional visible-light-emitting D–A systems, for which the photovoltaic parameters are summarized in Supplementary Table 1 and EQE_{PV} and electroluminescence spectra are shown in Supplementary Fig. 3. From the electroluminescence and EQE_{PV} spectra we obtain E_{CT} and the reorganization energy by Gaussian fits, following a method outlined previously[19]. As indicated in Fig. 1b–d, E_{CT} corresponds to the intersection point of the appropriately normalized reduced EQE_{PV} and electroluminescence spectra[19].

As demonstrated with the BF-DPB:B4PYMPM device, efficient charge-carrier generation under illumination and efficient CT emission do not need to be mutually exclusive properties. Indeed, this device has a photovoltaic internal quantum efficiency (IQE_{PV}) of 83%, a FF of 70% and an EQE_{EL} of 1.5% (Supplementary Figs. 1 and 2 and Supplementary Table 1). The significantly lower IQE_{PV} and FF for the TmPPPyTz devices as compared to those containing B4PYMPM are due to more strongly bound CT states in the former, as will be shown in the following. We obtain deeper insights into the energetics of the CT states with respect to the energy of free charge carriers by performing temperature-dependent measurements of V_{oc} at different light intensities (suns–V_{oc} measurements). The photogenerated current density at a specific incident illumination intensity (J_{ph}) is linked to V_{oc} and temperature (T) by the Shockley equation for open-circuit conditions[23]:

$$J_{ph} = J_{00}\exp\left[\frac{eV_{oc} - E_{A,PV}}{n_{id}k_BT}\right] \quad (1)$$

where $E_{A,PV}$ is the activation energy for recombination corresponding to the value of eV_{oc} extrapolated to $T = 0$ K, J_{00} is the maximum theoretical recombination current, n_{id} the diode ideality factor and k_B the Boltzmann constant. Figure 2a–c shows three exemplary temperature-dependent suns–V_{oc} measurements for DCV5T-Me:C_{60}, BF-DPB:TmPPPyTz and BF-DPB:B4PYMPM (coloured lines). The orange lines in the side panels of Fig. 2a–c correspond to $E_{A,PV}$, which is the average of values determined using equation (1) at various illumination intensities. The fact that $E_{A,PV}$ is nearly independent of the illumination intensity proves the validity of equation (1). The deviations at low intensities are caused by an increased influence of the shunt resistance, which becomes more pronounced at high temperatures[24]. For DCV5T-Me:C_{60}, $E_{A,PV}$ has a value of 1.39 eV, which is slightly lower than its E_{CT} of 1.47 eV (Fig. 2a). In contrast, for BF-DPB:TmPPPyTz, $E_{A,PV}$ lies ~0.15 eV above E_{CT} (Fig. 2b), while for BF-DPB:B4PYMPM, $E_{A,PV}$ equals E_{CT} within 0.01 eV.

The activation energy of the emitted light intensity $E_{A,EL}$ behaves in a similar manner to $E_{A,PV}$, resulting in an equation analogous to equation (1) for the emitted photon flux ϕ at low injection currents:

$$\phi = \phi_{00}\exp\left[\frac{eV - E_{A,EL}}{k_BT}\right] \quad (2)$$

where ϕ_{00} is the maximum theoretical photon flux. Photon flux versus voltage measurements at different temperatures as well as the extracted $E_{A,EL}$ values are shown in Fig. 2d–f. Note that $E_{A,PV}$ and $E_{A,EL}$ are equal to each other within 0.07 eV for small injection currents. Therefore, in the remainder of the text we denote $E_A \approx E_{A,PV} \approx E_{A,EL}$. All values are summarized in Supplementary Table 1, including further D materials in combination with TmPPPyTz and B4PYMPM (for their temperature-dependent analysis see Supplementary Figs. 4 and 6). In general, we find the following correlation: high-FF devices exhibit E_A smaller or equal to E_{CT}, while for poor FF devices E_A is significantly larger than E_{CT}. In what follows, we will rationalize this observation and will show that $E_A - E_{CT}$ is a good measure for the CT state binding energy. Consider therefore the electronic processes regulating the conversion of CT states at energy E_{CT} into free charge carriers at energy E_{FC} and vice versa.

In the case where the CT state is strongly bound, every free electron–hole encounter will result in CT state decay, independent of the value of E_{CT}. One can derive, in that case, that $E_A = E_{FC}$, making $E_A - E_{CT}$ equal to the CT state binding energy[12]. When TmPPPyTz is used as acceptor, $E_A - E_{CT}$ is larger than a few k_BT and the FF and IQE_{PV} values are indeed significantly reduced (Supplementary Table 1), because in this case CT state (re-)dissociation is a very rare process. Accordingly, the lifetime of the CT state is determined by the CT state decay rate only, while the lifetime of the free carriers is determined by their encounter rate. Often, these assumptions are made implicitly for OLEDs, but, as shown below, they are not correct for the B4PYMPM-containing devices studied[25].

If CT state dissociation occurs much faster than CT state decay, free carriers and CT states are transformed into each other several times before CT state decay. One can derive that $E_A = E_{CT}$ and the populations of free carriers and CT states decay at the same overall rate[12]. Such an equilibrium of CT states and free carriers before decay is a prerequisite for efficient photocurrent generation and high FF values. This is consistent with the fact that devices containing C_{60} and B4PYMPM as acceptor have good photovoltaic characteristics (Fig. 1e,g) and E_A is not substantially higher than E_{CT}. Furthermore, as the onset voltages for electroluminescence emission are in this case determined by E_{CT} instead of E_{FC}, they can be substantially reduced. Indeed the onset for electroluminescence emission occurs for BF-DPB:B4PYMPM ($E_A \approx E_{CT}$) at ~0.2 eV lower than for BF-DPB:TmPPPyTz ($E_A - E_{CT} \approx 0.2$ eV), even though E_{CT} is rather similar in these systems (Fig. 2e,f).

The beneficial properties of B4PYMPM with respect to free carrier photogeneration and the associated low onset voltage for emission are probably associated with the ability of B4PYMPM to form molecular stacks with a rather high charge carrier mobility, providing pathways for CT states to dissociate[26]. Indeed, when using B3PYMPM, a very similar molecule to B4PYMPM but with much less tendency to stack[26], we find a significant CT state binding energy, as well as a reduced photovoltaic performance and a substantially lower FF (Supplementary Figs. 7 and 8).

The visible-light-emitting devices studied in this work have a 1,000 to 10,000 times higher EQE_{EL} than typical OSC blends[3,27], irrespective of their charge generating properties and CT state binding energy. This results in about 0.20 V reduction in the non-radiative voltage losses (ΔV_{nr}) which are related to the EQE_{EL} by[3]

$$\Delta V_{nr} = \frac{k_BT}{e}\ln\left(\frac{1}{EQE_{EL}}\right) \quad (3)$$

In the concrete examples of BF-DPB:TmPPPyTz and BF-DPB:B4PYMPM, ΔV_{nr} is 0.09 V and 0.10 V, resulting in $E_{CT} - eV_{oc}$ differences of 0.37 eV and 0.45 eV, respectively. For DCV5T-Me:C_{60}, a significantly higher ΔV_{nr} of 0.29 V and $E_{CT} - eV_{oc}$ of 0.53 eV are found, which are typical for current state-of-the-art OSCs[3,4,28]. Figure 3 plots V_{oc}, ΔV_{nr} and EQE_{EL} as a function of E_{CT}. Previously published data on fullerene-containing OSCs[3] are supplemented by data for vacuum and solution-processed devices based on non-fullerene acceptors (NFAs), including the high-E_{CT} devices discussed above. Also, with the addition of these new devices, a trend where ΔV_{nr} decreases with increasing E_{CT} can be observed. This prevailing trend therefore indicates that non-radiative decay in fullerene and non-fullerene-based D–A devices is intrinsically linked to electron–phonon coupling[3]. These findings are in accordance with the energy-gap law, which describes that in organic molecules the non-radiative decay rate is

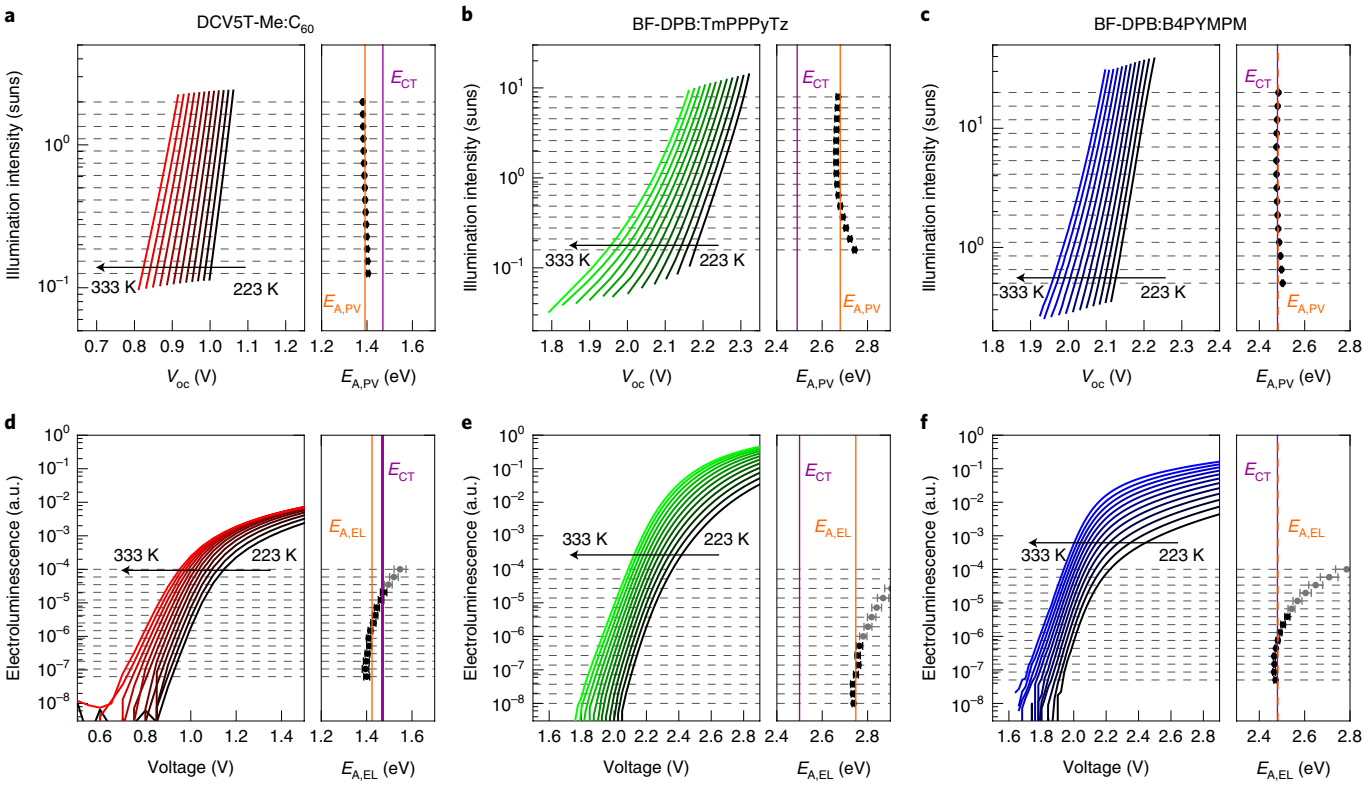

Fig. 2 | Temperature-dependent V_{oc} and the EL measurements. **a**–**c**, Top row, temperature-dependent suns-V_{oc} measurements of DCV5T-Me:C_{60} (**a**), BF-DPB:TmPPPyTz (**b**) and BF-DPB:B4PYMPM (**c**). **d**–**f**, Bottom row, temperature-dependent electroluminescence measurements of DCV5T-Me:C_{60} (**d**), BF-DPB:TmPPPyTz (**e**) and BF-DPB:B4PYMPM (**f**). In all measurements, the temperature was varied between 223 K and 333 K in steps of 10 K, as indicated by the black arrow. Grey dashed lines indicate fixed light intensities or emitted photon counts at which the voltage is taken as a function of temperature and extrapolated to 0 K. The corresponding fitted activation energies $E_{A,PV}$ and $E_{A,EL}$ are shown in the side panels as dots, with the error bars corresponding to fitting error. For activation energies with fitting errors smaller than 15 meV the average is taken and indicated by a vertical orange line. Fits are shown in Supplementary Fig. 5. The optically determined E_{CT} is plotted as a purple vertical line.

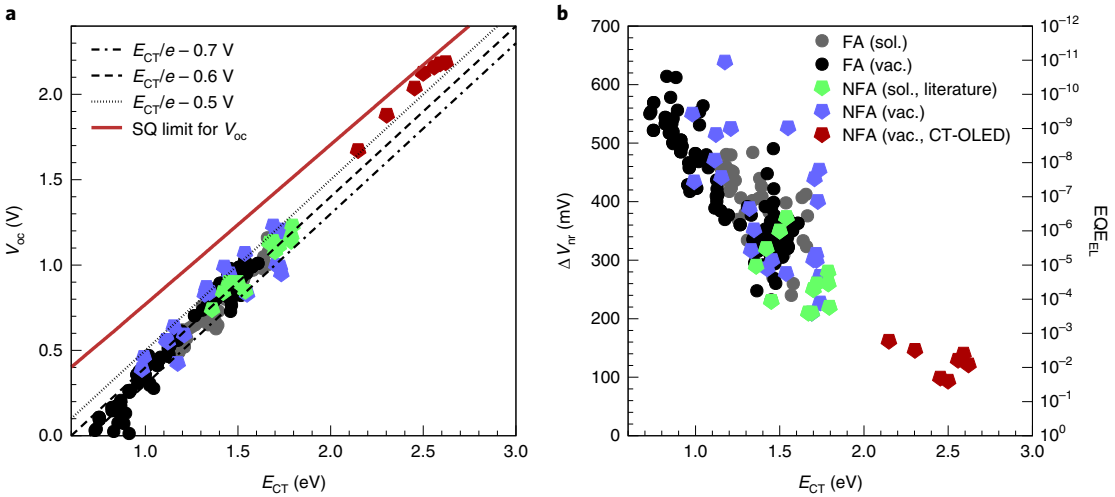

Fig. 3 | Open-circuit voltage and non-radiative voltage losses as a function of E_{CT}. **a**,**b**, V_{oc} (**a**), ΔV_{nr} and EQE_{EL} (**b**) as a function of E_{CT} for more than 170 different OSCs based on fullerene (FA) (circles) or NFAs (pentagons). Devices processed from solution are represented by grey and green symbols; all the others are processed by evaporation. Data shown by grey, light-green and black symbols were published previously[3,4,27,28,32–36]. CT-OLED devices discussed in this publication are shown in red. Details for all devices are provided in Supplementary Table 3.

exponentially decreasing with the energy difference between electronically excited state and ground state[3,29]. The devices discussed above extend the analysis to E_{CT} values in the visible region of the electromagnetic spectrum. Only for these high-E_{CT} devices do we find significantly reduced voltage losses and EQE_{EL} values of about 1%, bringing them closer to their theoretical maximum V_{oc} as given

by the Shockley–Queisser (SQ) limit (Fig. 3a). For the set of data plotted in Fig. 3b, a small deviation from the approximately linear relation of $\Delta V_{nr} \propto E_{CT}$ can be observed. These are probably caused by a variation of the molecular parameters influencing the energy-gap law[30]. Nevertheless, the impressive span of the trend between ΔV_{nr} and E_{CT} for a large energy range indicates that the main figure of merit substantially altering the non-radiative decay is plainly found in the value of E_{CT}. Details of the chemical structures of D and A are of secondary importance, as we find for both fullerene- and NFA-containing OSCs non-radiative voltage losses within the same range for a given E_{CT}.

We conclude this work by pointing out that we have found visible-light-emitting D–A systems with voltage losses $E_{CT} - eV_{oc}$ as low as 0.37 eV. This value is severely reduced compared to the typical values of 0.60 eV for OSCs, and approaches the voltage losses of GaAs of 0.32 eV (ref. [31]). This is the direct consequence of decreasing non-radiative decay pathways, resulting in EQE_{EL} values in the percent range. However, in the particular case of the BF-DPB:TmPPPyTz blend, temperature-dependent measurements show that the CT state has a binding energy of ~0.15–0.20 eV, resulting in a reduced FF and IQE_{PV}. In contrast, we demonstrate that for a BF-DPB:B4PYMPM blend with a similar CT state energy of 2.49 eV, the CT emission quantum yield is 1,000–10,000 times higher than for typical OSC materials, while the FF of 70% and IQE_{PV} of 83% are comparable to well performing OSCs. This work therefore shows that efficient photogeneration of free carriers and a high electroluminescence quantum yield do not necessarily need to be mutually exclusive in organic semiconductors. The resulting reduced non-radiative voltage losses, on par with or even below those of inorganic technologies, make visible-light-emitting D–A systems interesting for an efficient capture and low-energy-loss conversion of visible photons in photovoltaics, for example for indoor application and multijunction solar cells.

Online content

Any methods, additional references, Nature Research reporting summaries, source data, statements of data availability and associated accession codes are available at https://doi.org/10.1038/s41563-019-0324-5.

Received: 25 September 2018; Accepted: 19 February 2019;
Published online: 1 April 2019

References

1. Yan, C. et al. Non-fullerene acceptors for organic solar cells. *Nat. Rev. Mater.* **3**, 18003 (2018).
2. Sarma, M. & Wong, K.-T. Exciplex: an intermolecular charge-transfer approach for TADF. *ACS Appl. Mater. Interfaces* **10**, 19279–19304 (2018).
3. Benduhn, J. et al. Intrinsic non-radiative voltage losses in fullerene-based organic solar cells. *Nat. Energy* **2**, 17053 (2017).
4. Qian, D. et al. Design rules for minimizing voltage losses in high-efficiency organic solar cells. *Nat. Mater.* **17**, 703–709 (2018).
5. Goushi, K., Yoshida, K., Sato, K. & Adachi, C. Organic light-emitting diodes employing efficient reverse intersystem crossing for triplet-to-singlet state conversion. *Nat. Photon.* **6**, 253–258 (2012).
6. Chen, D. et al. Fluorescent organic planar pn heterojunction light-emitting diodes with simplified structure, extremely low driving voltage, and high efficiency. *Adv. Mater.* **28**, 239–244 (2016).
7. Lin, T.-C. et al. Probe exciplex structure of highly efficient thermally activated delayed fluorescence organic light emitting diodes. *Nat. Commun.* **9**, 3111 (2018).
8. Davy, N. C. et al. Pairing of near-ultraviolet solar cells with electrochromic windows for smart management of the solar spectrum. *Nat. Energy* **2**, 17104 (2017).
9. Lungenschmied, C. et al. Flexible, long-lived, large-area, organic solar cells. *Sol. Energy Mater. Sol. Cells* **91**, 379–384 (2007).
10. Meerheim, R., Körner, C. & Leo, K. Highly efficient organic multi-junction solar cells with a thiophene based donor material. *Appl. Phys. Lett.* **105**, 063306 (2014).
11. Meng, L. et al. Organic and solution-processed tandem solar cells with 17.3% efficiency. *Science* **6407**, 1094–1098 (2018).
12. Vandewal, K. Interfacial charge transfer states in condensed phase systems. *Annu. Rev. Phys. Chem.* **67**, 113–133 (2016).
13. Liu, X. K. et al. Prediction and design of efficient exciplex emitters for high-efficiency, thermally activated delayed-fluorescence organic light-emitting diodes. *Adv. Mater.* **27**, 2378–2383 (2015).
14. Chang, W. et al. Spin-dependent charge transfer state design rules in organic photovoltaics. *Nat. Commun.* **6**, 6415 (2015).
15. Attar, Aa. H. A. & Monkman, A. P. Electric field induce blue shift and intensity enhancement in 2D exciplex organic light emitting diodes; controlling electron–hole separation. *Adv. Mater.* **28**, 8014–8020 (2016).
16. Jenekhe, S. A. & Osaheni, J. A. Excimers and exciplexes of conjugated polymers. *Science* **265**, 765–768 (1994).
17. Vandewal, K. et al. Efficient charge generation by relaxed charge-transfer states at organic interfaces. *Nat. Mater.* **13**, 63–68 (2014).
18. Park, S. H. et al. Bulk heterojunction solar cells with internal quantum efficiency approaching 100%. *Nat. Photon.* **3**, 297–303 (2009).
19. Vandewal, K., Tvingstedt, K., Gadisa, A., Inganäs, O. & Manca, J. V. Relating the open-circuit voltage to interface molecular properties of donor:acceptor bulk heterojunction solar cells. *Phys. Rev. B* **81**, 125204 (2010).
20. Tvingstedt, K. et al. Radiative efficiency of lead iodide based perovskite solar cells. *Nat. Sci. Rep.* **4**, 6071 (2014).
21. Rau, U. Reciprocity relation between photovoltaic quantum efficiency and electroluminescent emission of solar cells. *Phys. Rev. B* **76**, 085303 (2007).
22. McNaught, A. D. & Wilkinson, A. *IUPAC Compendium of Chemical Terminology* 2nd edn (Blackwell Scientific, 1997).
23. Tvingstedt, K. & Deibel, C. Temperature dependence of ideality factors in organic solar cells and the relation to radiative efficiency. *Adv. Energy Mater.* **6**, 1502230 (2016).
24. Banerjee, S. & Anderson, W. A. Temperature dependence of shunt resistance in photovoltaic devices. *Appl. Phys. Lett.* **49**, 38–40 (1986).
25. Santos, Da. P. L., Dias, F. B. & Monkman, A. P. Investigation of the mechanisms giving rise to TADF in exciplex states. *J. Phys. Chem. C* **120**, 18259–18267 (2016).
26. Yokoyama, D., Sasabe, H., Furukawa, Y., Adachi, C. & Kido, J. Molecular stacking induced by intermolecular C–HN hydrogen bonds leading to high carrier mobility in vacuum-deposited organic films. *Adv. Funct. Mater.* **21**, 1375–1382 (2011).
27. Liu, J. et al. Fast charge separation in a non-fullerene organic solar cell with a small driving force. *Nat. Energy* **1**, 16089 (2016).
28. Liu, X. et al. Efficient organic solar cells with extremely high open-circuit voltages and low voltage losses by suppressing nonradiative recombination losses. *Adv. Energy Mater.* **9**, 1801699 (2018).
29. Englman, R. & Jortner, J. The energy gap law for radiationless transitions in large molecules. *Mol. Phys.* **18**, 145–164 (1970).
30. Azzouzi, M. et al. Nonradiative energy losses in bulk-heterojunction organic photovoltaics. *Phys. Rev. X* **8**, 31055 (2018).
31. Kayes, B. M. et al. 27.6% conversion efficiency, a new record for single-junction solar cells under 1 sun illumination. In *IEEE Photovoltaic Specialists Conference* (IEEE, 2011).
32. Zhang, J. et al. Efficient non-fullerene organic solar cells employing sequentially deposited donor–acceptor layers. *J. Mater. Chem. A* **6**, 18225–18233 (2018).
33. Yang, D. et al. A minimal non-radiative recombination loss for efficient non-fullerene all-small-molecule organic solar cells with a low energy loss of 0.54 eV and high open-circuit voltage of 1.15 V. *J. Mater. Chem. A* **6**, 13918–13924 (2018).
34. Tang, Z. et al. A new fullerene-free bulk-heterojunction system for efficient high-voltage and high-fill factor solution-processed organic photovoltaics. *Adv. Mater.* **27**, 1900–1907 (2015).
35. Nikolis, V. C. et al. Reducing voltage losses in cascade organic solar cells while maintaining high external quantum efficiencies. *Adv. Energy Mater.* **7**, 1700855 (2017).
36. Zhao, W. et al. Fullerene-free polymer solar cells with over 11% efficiency. *Adv. Mater.* **28**, 4734–4739 (2016).

Acknowledgements

This work was supported by the German Federal Ministry for Education and Research (BMBF) through the InnoProfile project 'Organische p–i–n Bauelemente 2.2' (03IPT602X) and by the German Research Foundation (DFG) project Photogen (VA 1035/5-1). X.J. and Y.L. acknowledge support from the China Scholarship Council (nos. 201706140127 and 201506920047, respectively). The authors also acknowledge the DFG for supporting K.T. (project 382633022 'RECOLPER'), F.P., S.Ro. and D.N. (SFB 951 'HIOS') and A.F. (RE 3198/6-1 'EFOD').

Author contributions

S.U., J.B., X.J., D.S. and K.V. designed the experiments, prepared photovoltaic devices and optimized their processing parameters for photovoltaic performance. S.U., X.J., Y.L. and J.W. performed temperature-dependent characterization of the devices.

J.B. and X.J. measured the sensitive EQE_{PV} spectra. K.T., V.C.N., F.P. and S.Ro. measured the EQE_{EL} and corresponding electroluminescence spectra. D.N., A.F., S.Re. and K.V. supervised sub-tasks (OPV and OLED design, investigation and data interpretation) within the project and participated in discussions of the findings. K.V. supervised the overall project. All authors contributed to the data analysis and writing of the manuscript.

Competing interests

The authors declare no competing interests.

Additional information

Supplementary information is available for this paper at https://doi.org/10.1038/s41563-019-0324-5.

Reprints and permissions information is available at www.nature.com/reprints.

Correspondence and requests for materials should be addressed to S.U., J.B. or K.V.

Publisher's note: Springer Nature remains neutral with regard to jurisdictional claims in published maps and institutional affiliations.

Methods

Device preparation. The layers of the OSCs were thermally evaporated at ultrahigh vacuum (base pressure of $<10^{-7}$ mbar) on a glass substrate with a pre-structured indium tin oxide (ITO) contact (Thin Film Devices). Glass substrates were cleaned in a multistep wet process including rinsing with *N*-methyl-2-pyrrolidone, ethanol and deionized water as well as treatment with ultraviolet ozone. Details on the layer sequence for each device are listed in Supplementary Table 2. We tested different hole transport layers for the high-gap devices; the results are listed in Supplementary Table 4. All organic materials were purified two to three times by sublimation. The device area was defined by the geometrical overlap of the bottom and the top contact and was equal to 6.44 mm^2. To avoid exposure to ambient conditions, the organic part of the device was covered by a small glass substrate, which was glued on top.

Current–voltage characteristics. Current–voltage characteristics in the dark and under solar illumination were measured with a Keithley 2400 SMU source meter at room temperature in ambient conditions. The cells are illuminated with a spectrally mismatch-corrected intensity of 100 mW cm^{-2} (AM1.5G) provided by a sun simulator (16S–150V.3, Solar Light Co.). Masks were used to minimize edge effects and to define an exact photoactive area (2.78 mm^2). The intensity was monitored with a Hamamatsu S1337 silicon photodiode (calibrated by Fraunhofer ISE Freiburg). Light-intensity-dependent FF measurements of the CT-OLEDs were conducted using three 385 nm APG2C1-385-r2 ultraviolet light-emitting diodes (LEDs, Roithner) in series as the illumination source and a Keithley SMU 2635A to measure the current–voltage curve.

EQE_{PV} measurements. EQE_{PV} measurements were performed according to previous works, reproduced here for completeness[3,10]. EQE_{PV} was measured using masks to minimize edge effects and to define an exact photoactive area (2.78 mm^2). The EQE_{PV} was detected with a lock-in amplifier (Signal Recovery SR 7265) under monochromatic illumination (Oriel Xe Arc-Lamp Apex Illuminator combined with Cornerstone 260 1/4 m monochromator) using a calibrated monocrystalline silicon reference diode (Hamamatsu S1337 calibrated by Fraunhofer ISE). For sensitively measured EQE_{PV} the light of a quartz halogen lamp (50 W) was used for low-E_{CT} devices or a white high-power LED (LED Engin LZP-00CW00) for the high-E_{CT} devices, chopped at 140 Hz and coupled into a monochromator (Newport Cornerstone 260 1/4 m). The resulting monochromatic light was focused onto the OSC, and its current under short-circuit conditions was fed to a current preamplifier before it was analysed with a lock-in amplifier (Signal Recovery 7280 DSP). The time constant of the lock-in amplifier was chosen to be 1 s and the amplification of the preamplifier was increased to resolve low photocurrents. The EQE_{PV} was determined by dividing the photocurrent of the OSC by the flux of incoming photons, which was measured using a calibrated Si and InGaAs photodiode (FDS100-CAL and FGA21-CAL, Thorlabs).

Electroluminescence measurements. Electroluminescence measurements were performed according to previous work, reproduced here for completeness[37]. The electroluminescence spectra were obtained with an Andor SR393i-B spectrometer equipped with a cooled Si and cooled InGaAs charge-coupled device (CCD) detector array (DU420A-BR-DD and DU491A-1.7). The spectral response of the set-up was calibrated with a reference lamp (Oriel 63355). The emission spectrum of the OSCs was recorded at different injection currents with respect to voltages, which were lower than or at least similar to the V_{oc} of the device at 1 sun illumination. Additional certification of the electroluminescence measurements was determined by a flux-calibrated Acton SpectraPro SP2560 monochromator coupled to a cooled Spec10LN Si CCD camera from Princeton Instruments.

EQE_{EL} measurements. EQE_{EL} measurements were performed according to previous work, reproduced here for completeness[3]. The EQE_{EL} was measured by forward biasing the OSCs with either an Agilent 4155C parameter analyser or Keithley SMU and collecting the emitted radiation with an enhanced G10899-03K InGaAs photodetector from Hamamatsu. The absolute total photon flux determination was performed by placing the OSC at a distance of 18.3 mm from the photodetector. Knowledge about the spectral distribution of the cell emission, the spectral response of the InGaAs photodetector and the assumption of a point source emitting uniformly into a half-sphere allows for determination of the absolute electroluminescence photon flux from the OSC. Uncertainties in the measured EQE_{EL} are expected to be governed by the small distance imprecision between the OSC and the photodetector (calibrated Si detector from Newport, 818 series with an active area of 1 cm^2). To keep this uncertainty as small as possible, measurements were conducted at different distances from the solar cell and always extrapolated to the full half sphere.

Temperature-dependent suns–V_{oc} and electroluminescence measurements. Measurements were conducted with a home-made set-up. For suns–V_{oc} measurements, a Keithley SMU2635A controlled the LED (a white LED (APG2C3-NW, Roithner) for the OSCs and a 365 nm LED (APG2C1-365-r4, Roithner) for the CT-OLEDs) to change the light intensity. A Keithley dual-channel SMU2602A was used to measure both the V_{oc} and the illumination intensity with a Newport 818-UV photodiode. To measure the electroluminescence, the dual-channel SMU2602A applied a bias voltage to the sample and measured the photocurrent of a S2387-66R Si photodiode (Hamamatsu), which was directly attached to the device, covering the whole active area. To change the cell temperature, the devices were placed in vacuum on a copper block, which was connected to a Peltier element (Peltron), controlled by a BelektroniG HAT Control device.
The measurement equipment was controlled with the software SweepMe! (https://sweep-me.net).

Determination of IQE_{PV}. The IQE_{PV} of the investigated devices was obtained by dividing the experimental EQE_{PV} by the simulated absorption of the active layer of each device. Optical simulations were performed using a numerical code based on the transfer matrix method, which uses the refractive index n, extinction coefficient k and the layer thickness to calculate the photon absorption and the distribution of the optical field within the solar cell. Variable-angle spectroscopic ellipsometry was performed to determine the n and k values of the active layers (BF-DPB:TmPPPyTz and BF-DPB:B4PYMPM) utilizing an EP4 imaging ellipsometer (Accurion GmbH). The ellipsometric parameters Ψ and Δ of 50-nm-thick layers on quartz glass substrates were measured for two different angles of incidence (50° and 60°) in a wavelength range from 360 nm to 700 nm and were approximated with an isotropic model containing two Gaussian oscillators.

Reporting summary. Further information on research design is available in the Nature Research Reporting Summary linked to this article.

Data availability

The data that support the plots within this paper and other findings of this study are available from the corresponding authors upon reasonable request.

References

37. Benduhn, J. et al. Impact of triplet excited states on the open-circuit voltage of organic solar cells. *Adv. Energy Mater.* **8**, 1800451 (2018).

nature research

Corresponding author(s): K. Vandewal, S. Ullbrich, J. Benduhn

Solar Cells Reporting Summary

Nature Research wishes to improve the reproducibility of the work that we publish. This form is intended for publication with all accepted papers reporting the characterization of photovoltaic devices and provides structure for consistency and transparency in reporting. Some list items might not apply to an individual manuscript, but all fields must be completed for clarity.

For further information on Nature Research policies, including our data availability policy, see Authors & Referees.

Experimental design

Please check: are the following details reported in the manuscript?

1. Dimensions

Area of the tested solar cells	☒ Yes ☐ No	Method Section
Method used to determine the device area	☒ Yes ☐ No	Method Section

2. Current-voltage characterization

Current density-voltage (J-V) plots in both forward and backward direction	☐ Yes ☒ No	For organic small molecule solar cells it is not needed since no hysteresis effect is reported.
Voltage scan conditions *For instance: scan direction, speed, dwell times*	☐ Yes ☒ No	For organic small molecule solar cells it is not relevent since no hysteresis effect is reported.
Test environment *For instance: characterization temperature, in air or in glove box*	☒ Yes ☐ No	Method Section
Protocol for preconditioning of the device before its characterization	☐ Yes ☒ No	No preconditioning required since no hysteresis reported for organic small molecules.
Stability of the J-V characteristic *Verified with time evolution of the maximum power point or with the photocurrent at maximum power point; see ref. 7 for details.*	☐ Yes ☒ No	Organic small molecule solar cells are known to be stable.

3. Hysteresis or any other unusual behaviour

Description of the unusual behaviour observed during the characterization	☐ Yes ☒ No	No unsual behavior observed.
Related experimental data	☐ Yes ☒ No	Not needed, see above.

4. Efficiency

External quantum efficiency (EQE) or incident photons to current efficiency (IPCE)	☒ Yes ☐ No	Main text and supplementary information.
A comparison between the integrated response under the standard reference spectrum and the response measure under the simulator	☐ Yes ☒ No	Current-Voltage measurements are performed with mismatch corrected illumination spectra (see methods).
For tandem solar cells, the bias illumination and bias voltage used for each subcell	☐ Yes ☒ No	No tandem solar cells are included in this work.

5. Calibration

Light source and reference cell or sensor used for the characterization	☒ Yes ☐ No	Method Section
Confirmation that the reference cell was calibrated and certified	☒ Yes ☐ No	Method Section

Calculation of spectral mismatch between the reference cell and the devices under test	☒ Yes ☐ No	Method Section

6. Mask/aperture

Size of the mask/aperture used during testing	☒ Yes ☐ No	Method Section
Variation of the measured short-circuit current density with the mask/aperture area	☐ Yes ☒ No	Not relevant for the scope of the manuscript.

7. Performance certification

Identity of the independent certification laboratory that confirmed the photovoltaic performance	☐ Yes ☒ No	A certified PCE is not needed since the value is not relevant for the message of the paper.
A copy of any certificate(s) *Provide in Supplementary Information*	☐ Yes ☒ No	No performance certification.

8. Statistics

Number of solar cells tested	☒ Yes ☐ No	One device was characterized for each material composition (indicated in the SI).
Statistical analysis of the device performance	☐ Yes ☒ No	Vacuum processed solar cells are known to be very reproducible.

9. Long-term stability analysis

Type of analysis, bias conditions and environmental conditions *For instance: illumination type, temperature, atmosphere humidity, encapsulation method, preconditioning temperature*	☐ Yes ☒ No	Devices are encapsulated and long-term stability is not in the scope of the manuscript.